Nanoconfinement and Crowding Enhanced Single-molecule detection of small molecules with nanopipette.

Santosh Khatri¹, Popular Pandey¹, German Mejia^{2,3}, Govinda Ghimire¹, Fenfei Leng^{2,3}, Jin He^{1,3*}

¹Physics Department, Florida International University, Miami, Florida, 33199, USA

²Chemistry and Biochemistry Department, Florida International University, Miami, Florida, 33199, USA

³Biomolecular Science Institute, Florida International University, Miami, Florida, 33199, USA

Abstract

Glass nanopipette has gained widespread use as a versatile single-entity detector in chemical and biological sensing, analysis, and imaging. Its advantages include low cost, easy accessibility, simplicity of use, and high versatility. However, conventional nanopipettes based on the volume exclusion mechanism have limitations in detecting small biomolecules due to their small volume and high mobility in aqueous solution. To overcome this challenge, we have employed a novel approach by capitalizing on the strong nanoconfinement effect of nanopipette. This is achieved by utilizing both the hard confinement provided by the long taper nanopipette tip at the *cis* side and the soft confinement offered by the hydrogel at the *trans* side. Through this approach we have effectively slowed down the exit motion of small molecules, allowing us to enrich and jam them at the nanopipette tip. Consequently, we have achieved high throughput detection of small biomolecules with sizes as small as 1 nm, including nucleoside triphosphates, short peptides, and small proteins with excellent signal-to-noise ratios. Furthermore, molecular complex formation through specific intermolecular interactions, such as hydrogen bonding between closely spaced nucleotides in the jam-packed nanopipette tip, have been detected based on the unique ionic current changes.

Keywords: nanopipette, nanopore, nanoconfinement, molecular crowding, single-molecule detection, small molecule detection

Introduction

Nanopore sensing, originating from Coulter counter and single ion channel recording, has been widely used to detect, count, and analyze various biomolecules at the single-molecule level at the physiological conditions. The nanopore method has achieved remarkable success in DNA sequencing. Furthermore, it has been proven effective in detecting other biomolecules such as RNA and proteins. In recent years, glass or quartz nanopipettes, as a subtype of solid-state nanopores, have gained popularity for the detection of larger biomolecules and nanoparticles. Different from the conventional solid-state nanopores fabricated on ultrathin SiN or SiO membranes using focused electron or ion beams, an anopipettes can be prepared inexpensively, conveniently, and rapidly in any chemistry laboratory using a commercial pipette puller. However, it is still challenging to reliably pull nanopipette tips with nanopore sizes less than 10 nm. The radius of the nanopipette used for Nanoparticle detection in resistive-pulse sensing experiments should be approximately 1.5 to 3 times the radius of the translocating nano entity. Otherwise, the molecules translocate too fast to be reliably detected by the transient changes in ionic current using the current amplifier with the bandwidth of sub-millisecond. Therefore, there is still a significant obstacle in applying nanopipettes for the detection of small biomolecules.

To address this obstacle, one strategy inspired by nature is to introduce a crowding effect¹⁶ in the solution to slow down the motion of biomolecules during the translocation. We have employed the nanopipette based Di-electrophoresis (DEP) method¹⁷ to efficiently concentrate synthetic nanoparticles near the nanopipette tip, which introduces self-crowding near the nanopore entrance and leads to the obvious enhancement in the signal-to-noise ratio (SNR) and the event rate of current pulses.^{18,19} We hypothesize we may achieve high sensitivity for small biomolecules if we can induce self-crowding of small biomolecules near the nanopipette tip. However, the effectiveness of DEP force in trapping small molecules in the electrolyte is minimal due to its size dependence and short range.²⁰ Previous studies have shown that the addition of macromolecular crowding agents such as hydrogel or polymers in the solution can effectively slow down the translocation speed of biomolecules, leading to improved detection rate and SNR using solid-state nanopores on SiN or SiO₂ membranes.²¹⁻²⁵ By introducing crowding agents polyethylene glycol (PEG)²⁶ or hydrogel at the *trans* side,²⁷ the sensitivity and event rate of nanopipette for biomolecule detection are also enhanced. However, the previous work of using crowding agents did not

generate self-crowding of analytes near the nanopore and still could not detect label-free small biomolecules, including small proteins (≤ 100 amino acids (AAs)) and small molecules (≤ 1 kDa).

In this report, we present a facile approach (Figure 1a) to generate controllable crowding of small biomolecules near the nanopipette tip by combining the strong nanoconfinement effect of longtaper nanopipette tip and viscous hydrogel at the trans side. The molecule moves from the interior of the nanopipette barrel (cis side) to the bath filled with viscous hydrogel (trans side). The mobility of molecule is significantly reduced when entering the hydrogel, leading to a molecular jamming phenomenon near the nanopore. Interestingly, the induced self-crowding of biomolecules near the tip indeed greatly improves both the event rate and SNR for single-molecule detection. We demonstrate the ultrasensitive and highly effective detection of small biomolecules, including nucleoside triphosphates (<1 kDa), short peptides (a few kDa), and hormone insulin (5.8 kDa), with a high detection rate (over 100 s⁻¹) while using more than 15 times bigger size of the nanopore. The crowded environment also promotes specific intermolecular interactions, leading to the observation of nucleoside triphosphate complexes such as pairs and quadruplexes. The side effect of self-crowding of molecules at the tip is the more complex ionic signals. However, we demonstrate that these complex signals carry valuable information for molecular sensing and recognition. Consequently, this novel method opens exciting new opportunities for singlemolecule studies of small biomolecules.

Results and Discussion

Maximization of Nanoconfinement Effect to Induce Controllable Molecule Crowding

This approach employs the dual slowing mechanism provided by a long-taper nanopipette (see Figures 1a and 1b) at the *cis* side and viscous hydrogel at the *trans* side. The backend-loaded biomolecules are forced to pass a funnel-shaped long nanochannel before they exit from the nanopore orifice, which enhances the confinement effect of the nanochannel and slows down the biomolecules as they reach the orifice. To ensure a proper mass transport efficiency of molecules inside the nanopore barrel, we typically use a nanopipette with a nanopore diameter 5-15 times larger than the size of the molecules. For a molecule with a 2 nm hydrodynamic radius, its root mean square displacement of diffusion ($\sqrt{\langle r \rangle^2} = \sqrt{6Dt}$, D is the diffusion constant, t is the time) is over one micron in one millisecond in a three dimensional free space in 1xPBS at room

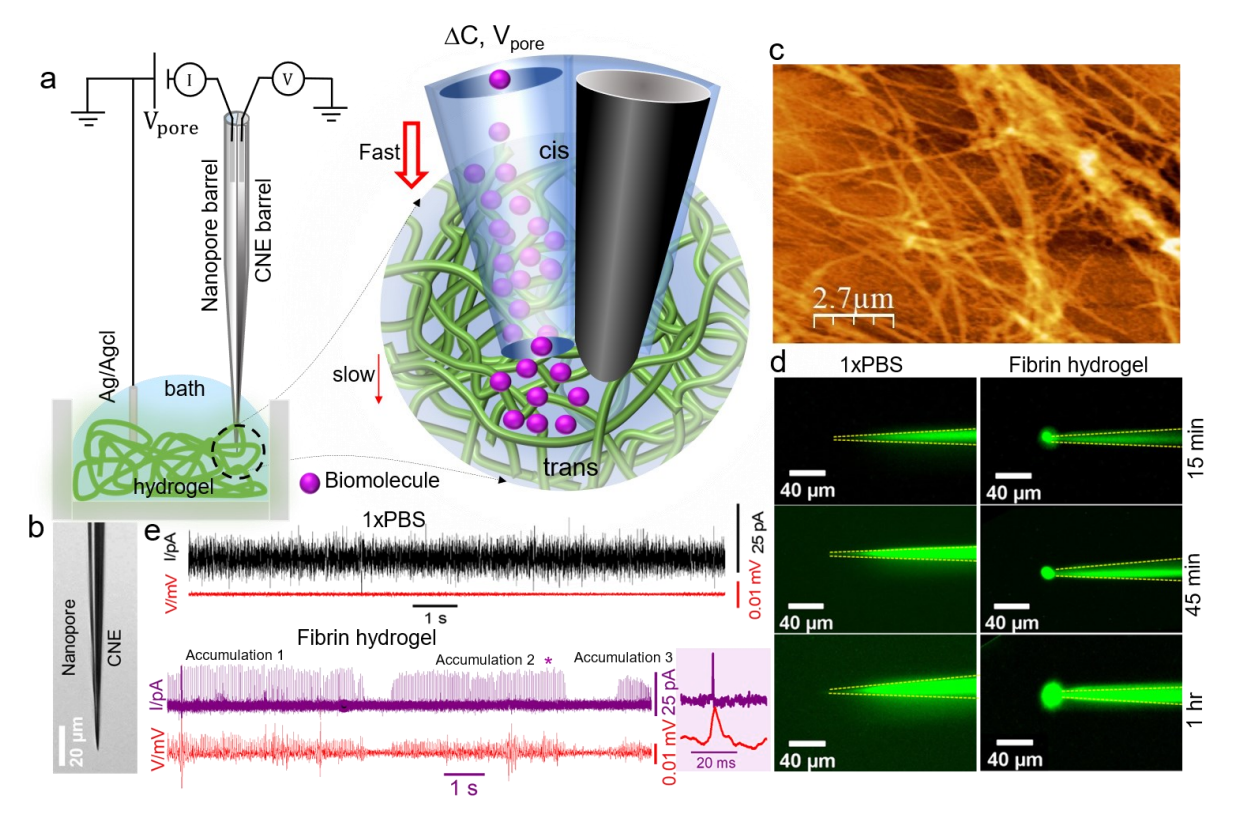


Figure 1. Experimental setup for small molecule detection through a nanopipette. a. An illustration of the experimental setup showing the accumulation of molecules at the nanopipette tip. b. An optical microscope image depicting the side view of a typical nanopipette tip. The dark side represents the CNE barrel filled with pyrolytic carbon. c. A tapping mode AFM topography image displaying the dried fibrin hydrogel on a mica surface. d. Fluorescence images of a nanopipette tip (nanopore size \sim 29 nm) in 1x PBS solution (left column) and fibrin hydrogel (right column) after loading 5 μ M FITC dye at -50 mV bias for 15 min, 45 min, and 1 hr. The yellow dashed lines indicate the outlines of the nanopipette tip. e. Top panel (bath solution is 1xPBS without fibrin hydrogel): typical *i-t* (black) and *v-t* (red) traces of insulin using a nanopipette with a nanopore diameter of \sim 19 nm. Bottom panel (bath solution is filled with fibrin hydrogel): typical *i-t* (purple) and *v-t* (red) traces after the accumulation of insulin at the tip of a nanopipette with a nanopore diameter of \sim 22 nm. The initial concentration of insulin is 500 pM and V_{pore} is zero. The *v-t* trace is filtered with a digital high pass filter (20 Hz) to remove the baseline fluctuations.

temperature. Therefore, the relatively bigger size of nanopore can still effectively confine the small molecules, suppressing their Brownian motion with a reduced entropy. Due to the confinement, we observed an increased sensitivity when the biomolecules were loaded inside the nanopore barrel compared to introducing them in the open bath solution. This is also consistent with the

previous report. Small biomolecules with sizes in the range of a few nanometers typically reach the tip in a few minutes through diffusion. The applied nanopore bias (V_{pore}) can further modulate the mass transport of small biomolecules through the nanopipette tip. However, the nanoconfinement from the long taper geometry of nanopipette tip is still not enough to contain many small molecules to form molecular jamming. We thus introduce viscous fibrin hydrogel outside the tip to provide a soft confinement and impede the exit of biomolecules from the nanopore. The viscosity of fibrin hydrogel is approximately 530 times higher than 1xPBS and nearly 5 times higher than the common macromolecule crowding agent PEG-8k solution with a 1:1 volume ratio²⁶ (Figure S2).

The accumulation of small molecules can be illustrated in the fluorescence experiments using FITC dye molecules (~ 1 nm in size) (see Figure 1d). In the bath solution without fibrin hydrogel, the fluorescence intensity near the tip remains low throughout the 1-hour measurement, suggesting the backloaded FITC dyes quickly diffuse out of the orifice and away from the tip. In contrast, with the hydrogel in the bath solution at the *trans* side, the fluorescence intensity near the tip increases obviously in 5 min, and then a high intensity spot was observed surrounding the tip (both at the *cis* and *trans* sides) after 15 min. The intensity near the tip increases continuously in the 1-hour measurement. Therefore, the hindered diffusion of FITC dyes leads to the accumulation of FITC dyes near the tip. It should be noted that the high viscosity of fibrin hydrogel is critical. For comparison, the bath solution mixed with PEG-8k is not viscous enough to induce the accumulation of small molecules (see Figure S5).

Insulin is a small protein (51 AAs) with a hydrodynamic radius (R_h) 1.4 nm (see table S1). Figure 1e illustrates representative current-time (*i-t*) traces for the detection of insulin with (purple trace) and without (black trace) the presence of fibrin hydrogel in the bath solution using nanopipettes with nanopore sizes approximately 7-8 times larger than that of insulin. Current spikes were only observed when fibrin hydrogel presented in the bath solution. The current spikes are from the translocation events of individual insulin molecules. The current spikes are highly concentrated (~34 s⁻¹) inside the cluster, which is due to the accumulation of insulin. Similar cluster formation was observed when nanoparticles are concentrated by the DEP force. ^{18, 19} These current spikes broke up into three clusters, revealing the accumulation-dissipation cycles at the tip. Typically, the numbers of spikes in these clusters become bigger and the gaps between clusters become smaller

with the increase of crowding level. It should be noted that the formation of insulin self-crowding at the tip is a result of the collective confinement effects exerted by both the nanopipette and fibrin hydrogel. The crowding of insulin is difficult to achieve when the nanopipette nanopore size is roughly doubled and about 15 times bigger than insulin (Figure S12). Corresponding transient changes have also been observed in the potential-time (*v-t*) traces (red) in Figure 1e. The translocation of negatively charged insulin induces open-circuit potential changes in the floating carbon nanoelectrode (CNE) near the nanopore (see Figures 1a and 1b). The potential changes acquired by CNE can provide useful complementary information. However, CNE is not necessary for this new approach. For example, similar phenomenon of insulin accumulation was observed using a single barrel nanopipette without CNE (Figure S6). To limit the scope of this paper, we only focus on the current changes and exclude the potential results below.

Self-crowding and Enhanced Detection of Short Peptides

Using this approach, we have tested 10 biomolecules with different R_h, D and mobility (see the full list in Tables S1-S3). While this approach also benefits the measurements of larger entities such as Ferritin and BSA (see Figure S7), it works exceptionally well for small biomolecules, which are generally challenging to detect. Due to their higher mobility, small biomolecules can accumulate in large numbers near the vicinity of the nanopore orifice within a brief period, even with small or zero V_{pore}. Figure 2 presents typical results for the negatively charged peptide micro peroxidase (MP-11) with 11 AAs and a Rh of 0.65 nm (Table S2). Similar results for a cationic antimicrobial peptide nisin (3.4 kDa) are also acquired (see Figure S8). The nanopipette tip with a nanopore size of ~16 nm, loaded with 100 pM MP-11, was initially placed in the bath solution (1x PBS) above the hydrogel. The *i-t* (black) trace is stable and featureless at zero bias (Figure 2a(i)). After lowering the nanopipette tip into the hydrogel, the *i-t* trace (see Figure 2a(ii)) remains stable and featureless. However, a significant reduction (~45%) in the noise level of the ionic current baseline has been observed in the hydrogel. The reduction in noise level with the nanopipette tip in fibrin hydrogel is attributed to reduced ion mobility, which decreases the 1/f noise.²⁹ Typically, after 5-10 min, we observed high-density upward current spikes in the *i-t* trace (see Figure 2a(iii)), which were indicative of individual MP-11 translocation events. Concurrently, the current baseline noise is further reduced by about 20% of the value in (ii). Comparing the noise levels in traces (i) and (iii), it became evident that MP-11 signals could not be detected in 1xPBS. The noise power spectral densities of traces (i)-(iii) also confirm the significant noise reduction (Figure S9). These

densely packed spikes suggest the enrichment of the MP-11 molecules at the tip. The increased local concentration of MP-11 in the confined nanopipette tip creates a strong volume exclusion effect, leading to reduced salt concentrations, suppressed Brownian motion, and slower translocation speed of MP-11. These factors further contributed to the noise reduction in the ionic current baseline. ²⁹ Like the insulin results in Figure 1e, the densely packed spikes appear in isolated clusters. The *i-t* traces in Figure 2b illustrate the formation of clusters at different V_{pore} values. Individual spikes in the cluster can be resolved in the zoom-in traces on the right side. The zoom-

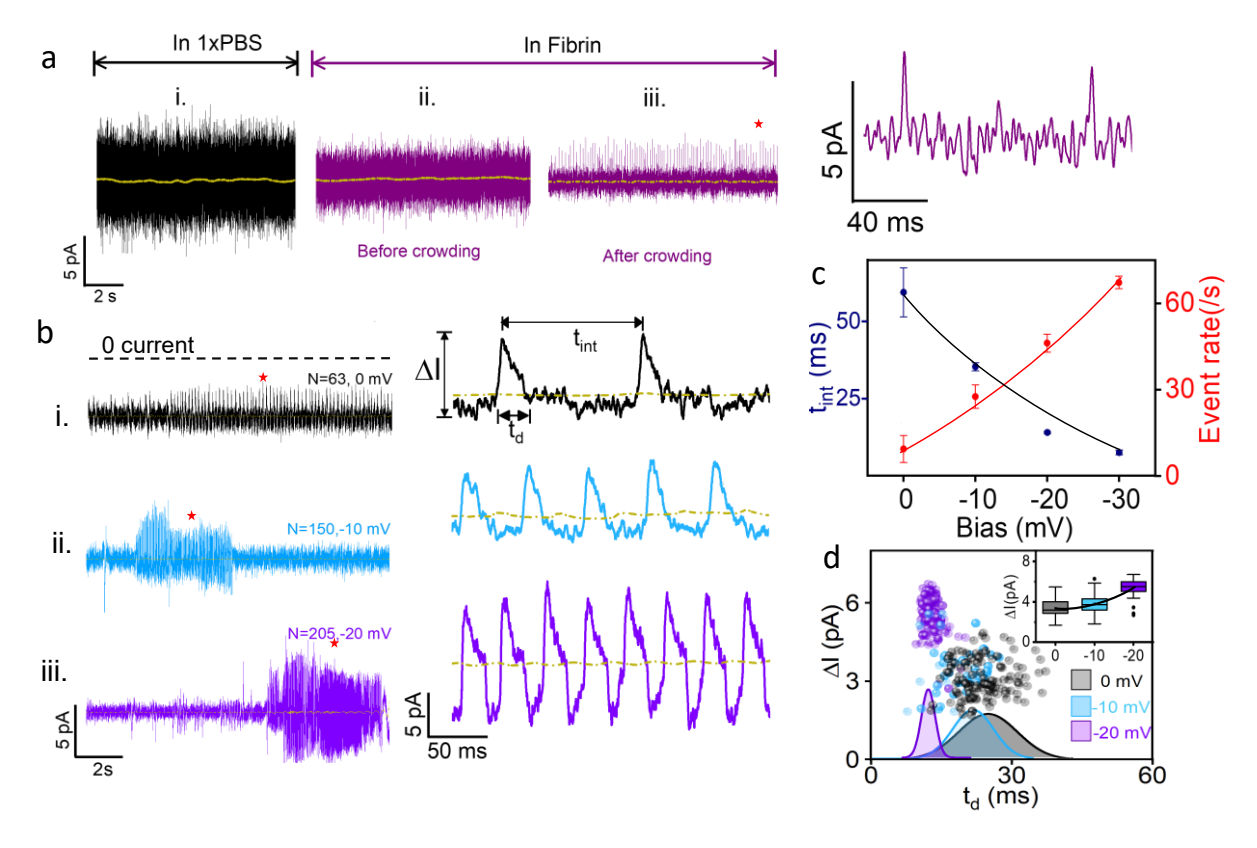


Figure 2. The detection of 100 pM MP-11. a. Representative *i-t* traces were obtained in 1xPBS (i), before (ii), and after (iii) molecule enrichment in fibrin hydrogel at -10 mV bias. The nanopipette with nanopore size of ~16 nm was used. The zoomed-in trace is from trace (iii) indicated by "*". b. Typical *i-t* traces showing the cluster formation of MP-11 at different V_{pore} in the presence of fibrin hydrogel. The black dash line represents the position of zero current, not drawn to scale. The brown dash line is the current baseline. Zoomed-in traces inside each cluster of traces in b. c. Plot showing the relationship between event rate and V_{pore} . For statistical analysis, event rate and event interval were calculated for at least 3 clusters. The solid lines serve as an eye guide. The data of -30 mV is shown in Figure S10. d. Scatter plots of ΔI *vs.* t_d at different V_{pore} values.

in traces are selected from the center of the clusters. Interestingly, the spikes are evenly spaced especially at -10 and -20 mV. In contrast, the time intervals (t_{int}) between two neighboring spikes are less uniform at the beginning and end of a cluster. The changes of t_{int} reveal that the internal structure of an MP-11 cluster is more organized, whereas the boundary exhibits less order. The ordered internal structure is further disrupted at the higher V_{pore} (i.e., -30 mV, Figure S10). Within each cluster, the total number and event rate of current spikes notably increases when the V_{pore} is more negative, accompanied by reduced t_{int} with bigger variations. As shown in Figure 2c, the mean event rate increased more than 9 times from nearly 7 $\rm s^{-1}$ to 63 $\rm s^{-1}$ with the $\rm V_{pore}$ from 0 mV to -30 mV. Meanwhile, the t_{int} dropped almost 7 times from nearly 59 ms to 8 ms. Therefore, the accumulation of MP-11 can be effectively controlled by the applied V_{pore} with a magnitude as small as tens of mV. The more negative V_{pore} induces more MP-11 to accumulate at the tip with a higher degree of crowding. Interestingly, we also observed the occurrence of current spikes and cluster formation even at a small positive V_{pore} (+10 mV) although the number of spikes in a cluster is much smaller. So, in the case of MP-11, the electrophoretic flow (EPF) generated by the small positive V_{pore} cannot fully cancel the diffusion flow of MP-11 and possible electroosmotic flow (EOF).

These spikes have asymmetric shapes, with a faster rising time and slower decay time. Asymmetric shape spikes have typically been observed when using asymmetric nanopores, such as track-etched conical nanopores in a polymer membrane³⁰ and glass/quartz nanopipettes,³¹ due to their asymmetric nanopore geometry and nonuniform local electric field distribution. However, we have found the asymmetric shapes of these spikes were also sensitive to the crowding level and often changed. These changes should reflect the dynamic crowding environment and will be further investigated. Furthermore, we have observed significant changes in the orientation of individual current spikes, transitioning from predominantly upward spikes of resistive events (REs) at zero bias to increasingly biphasic spikes of biphasic events (BEs) at -10 mV and -20 mV. Ultimately, the current spikes become downward of conductive events (CEs) at -30 mV bias. Previous works have shown that the transition from REs to BEs and CEs is associated with a decrease in local ion concentration, resulting in increased double-layer thickness, enhanced EOF, and ion concentration polarization.^{32,33,34} Therefore, these notable shape changes of the current spikes reveal the dramatic variations in local ion concentration induced by the self-crowding of MP-11 at the nanopipette tip. More notable shape changes of current spikes have often been observed for larger proteins, *i.e.*,

ferritin, due to their bigger volume to displace ions. As shown in Figure S11, the dynamic shape changes of current spikes are observed in one cluster at a constant V_{pore} . We observed the CEs in the middle but REs at the beginning and end of a dense cluster, reflecting a higher degree of crowding in the middle of a cluster.

We further studied the changes of duration (t_d) and peak height (ΔI) of individual current spikes with the change of local crowding level. We included both the upward and downward sections of the biphasic spikes when defining the t_d and ΔI , as illustrated in Figure 2b. There are some ambiguities in determining t_d and ΔI for the spikes of BEs because they are closely spaced and partially overlapped. Figure 2d presents the scatter plots of ΔI vs. t_d at different V_{pore} values. The distributions of t_d along with Gaussian fits as a function of V_{pore} are also shown in Figure 2d. As V_{pore} became more negative and the crowding level was higher, the distribution of t_d became narrower and its mean value decreased significantly, suggesting the faster translocation of MP-11 through the sensing zone. Meanwhile, the mean of ΔI increased with the more negative V_{pore} and thus the increased crowding level of MP-11 (see the inset of Figure 2d). The ΔI may also vary within a cluster, reflecting the non-uniformity of the crowding in a cluster. Typically, ΔI is slightly higher at the beginning of a cluster, revealing the higher local concentration of MP-11 at the front of a cluster. Interestingly, this is different from the case of larger proteins like ferritin.

Enhancing the Detection of Small proteins with Large Proteins

To further validate the idea of improving nanopipette sensitivity by the creation of molecule jamming, we introduce large non-interacting biomolecules as crowding agents within the nanopipette. This approach indeed works, and the pore-molecule size ratio can be further enlarged. One example is shown in Figure 3. Ferritin protein, with its mobility being over 20 times smaller than insulin (see table S3), was used as the crowding agent for insulin detection. In the experiment, a solution containing 500 pM ferritin was added to the nanopipette with a nanopore diameter of approximately 40 nm (almost 15 times bigger than the insulin size), and the mixture was left for approximately 2 hours. Since both ferritin and insulin are negative at neutral pH, a negative V_{pore} was applied to drive them electrophoretically toward the sensing zone of the nanopore. Upward current spikes corresponding to REs of individual translocating ferritin were observed with an event rate $\sim 14 \text{ s}^{-1}$ in the i-t trace at $\sim 30 \text{ mV}$ (see Figure 3a(i)).

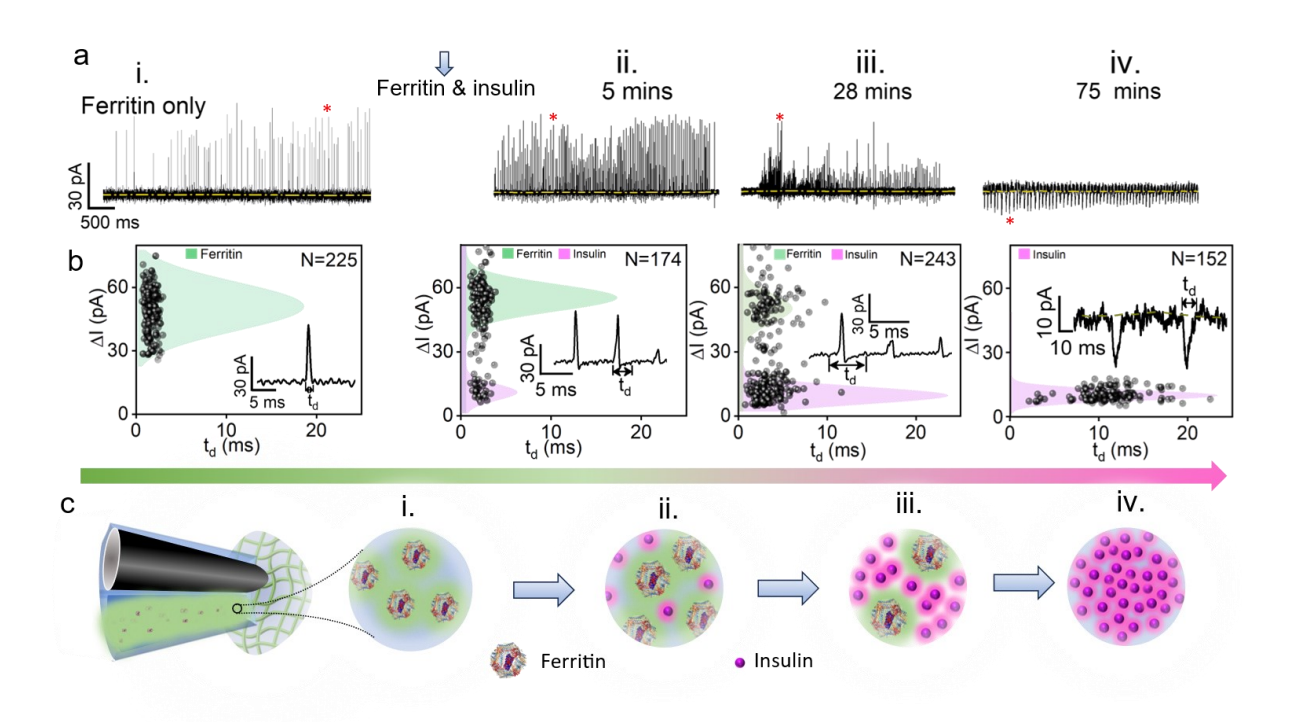


Figure 3. Detection of insulin using ferritin as the crowding agent. The V_{pore} is always -30 mV. The *cis* side inside the nanopore barrel is 1xPBS and the *trans* side is fibrin hydrogel. The size of the nanopore is ~40 nm. a. Representative *i-t* traces within an accumulated cluster at different time points: (i) the nanopore barrel is filled with 500 pM ferritin; (ii-iv) the nanopore barrel is filled with 250 pM ferritin and 250 pM insulin and after applying -30 mV for 5 min (ii), 28 min (iii) and 75 min. b. Corresponding scatter plots of ΔI (y-axis) *vs.* t_d (x-axis) for the current spike events appeared in the *i-t* traces. The shaded regions within each scatter plot represent the histogram of ΔI. The zoom-in *i-t* trace in each plot shows the representative current spikes with the definitions of ΔI and t_d . c. Schematic diagrams to illustrate the proposed crowding changes at the nanopipette tip.

The ΔI of these current spikes mostly fell within the 30-60 pA range, as depicted in Figure 3b(i). The scatter plot displays only one set of distributions. The ferritin solution within the nanopore barrel was subsequently replaced with the solution containing the mixture of ferritin and insulin both with 250 pM concentrations. The loaded nanopipette was left for about an hour before measurements. Figure 3a(ii) displays the *i-t* trace after applying -30 mV for 5 min. The event rate of current spikes is more than doubled (~34 s⁻¹) and the current baseline decreases slightly, suggesting a higher degree of crowding. In addition to the current spikes like the ones observed in Figure 3a(i), small upward spikes also appeared, as better illustrated in the inset in Figure 3b(ii).

The scatter plot in Figure 3b(ii) displays two distinct sets of distributions, indicating the presence of two different populations of proteins. The distribution of the large spikes closely resembles the ferritin distribution in Figure 3b(i). The smaller spikes, ranging in magnitude from 5-20 pA, were thus attributed to insulin. The ferritin spikes still dominated the recorded signals with a percentage of nearly 86%, which is attributed to the residual ferritin from the first load. The insulin from the second load have just reached the sensing zone at the tip (see Figure 3c(ii)).

Figure 3a(iii) depicts the *i-t* trace after applying -30 mV for 28 min with the second load. The event rate of current spikes remains high at 40 s⁻¹. The current spikes are nonuniform and two types of spikes are clearly visible. There are fewer large spikes with peak heights ~30-60 pA but more small spikes with peak heights ~10-20 pA. Furthermore, the spikes become slightly biphasic with a small dip following the large upward spike. The change in the spike shape reflects a decrease in local ion concentration and an increase in ion polarization resulting from the heightened local concentration of proteins. ³² The scatter plot in Figure 3b(iii) demonstrates that the percentage of small spikes (~75%) is significantly higher than the percentage of large spikes (25%). The t_d distributions for both ferritin and insulin become broader, attributed to the increased crowding at the tip and more collisions during molecule translocation. As shown in Figure 3c(iii), the smaller insulin, with higher mobility, gradually fills up the voids between large ferritin and replaces ferritin in the tip.

Figure 3a(iv) displays the *i-t* trace taken at nearly 75 min after the initial recording. Now the trace is densely occupied by small spikes with an event rate of 28 s⁻¹. The spikes are mostly downward (CEs). Additionally, we noted a decrease of about 10-14% in the magnitude of the current baseline. In Figure 3b(iv), only one set of distributions from insulin appears in the scatter plot. The distribution of t_d becomes very broad, and the mean of t_d obviously increases, suggesting the molecules move slow, which also lowers the event rate. All these changes suggest that the insulin has completely replaced the ferritin and that an increased accumulation of insulin near the tip has occurred (see Figure 3c(iv)). The results also show that insulin and ferritin can be fully separated based on their mobility difference in the nanopipette, revealing the non-interacting nature of the mixed molecules.

As we mentioned earlier, insulin can only be enriched and reliably detected when the nanopore size of the nanopipette is less than 20 nm and the pore-molecule size ratio is less than 10 (see

Figure 1e). If the size ratio exceeds 10, insulin is unable to be enriched and reliably detected (see Figure S12). Therefore, ferritin plays a critical role in enhancing the volume exclusion effect and facilitates the crowding of insulin. It is worth noting that besides ferritin, other larger proteins such as BSA can serve as the crowding agent to enhance the detection of insulin as well (see Figure S13).

Probing Intermolecular Interactions Between Nucleotide Triphosphates in a Crowded Environment

The jam-packed nanopipette tip should promote interactions between closely spaced molecules thus provide valuable opportunities to probe various interactions between small molecules in a crowded environment, like the cytoplasm of a living cell. Considering the well-understood hydrogen bonding interactions between nucleobases, we studied nucleoside triphosphates. Figures 4a-c display the results involving the mixture of adenosine triphosphate (ATP, 507 Da) with deoxycytidine triphosphate (dCTP, 467 Da). The initial i-t trace in Figure 4a(i) reveals frequent downward current spikes (CEs) with an event rate of 13 s⁻¹ following the accumulation of pure ATP. Subsequently, a solution of 100 pM dCTP was added to the nanopipette. As shown in trace (ii) of Figure 4a, more spikes with a higher event rate of 64 s⁻¹ are observed in trace (ii) than in trace (i) after 10 min of recording. The current spikes in trace (ii) show two distinct ΔI levels. At 35 min, trace (iii) is dominated by smaller spikes with a high event rate of 92 s⁻¹. Histogram (i) represents ATP alone and can be fitted by a single Gaussian distribution with a mean ΔI value of 11.3±4.7 pA. Histogram (ii) at 10 min can be fitted by two Gaussian peaks: one at 6.8±5.1 pA and the other at 12.8 ± 6.3 pA. Histogram (iii) at 35 min again can only be fitted by a single Gaussian peak at 6.6 \pm 2.5 pA. We assign small amplitude ΔI_1 to dCTP and big amplitude ΔI_2 to ATP (see the yellow shaded regions). The results remind us of the results in Figure 3 and manifest the weak interactions between ATP and dCTP. As illustrated in Figure 4c, the molecules accumulated at the tip changed from ATP to ATP/dCTP mixture and then to dCTP. Considering the well-known base pair complex between A and T nucleobases (see Figure 4e), we proceeded to investigate the mixture of ATP and deoxythymidine triphosphate (dTTP, 482 Da). Initially, we accumulated ATP at the tip and observed uniform downward peaks (CEs) in the i-t trace (i) of Figure 4d with an event rate of 97 s⁻¹. Correspondingly, we observed a single population with a mean value of 41.8±9.8 pA in the histogram (i) in Figure 4d. Here, the higher event rate than that

in Figure 4a(i) is due to the smaller pore size and a higher degree of crowding. Subsequently, we added dTTP and allowed them to accumulate at the tip for 15 min. As a result, the current spikes in trace (ii) (event rate of $104 \, \text{s}^{-1}$) became non-uniform, exhibiting spikes that can be divided into three ΔI levels. In the corresponding ΔI histogram (ii), the first peak was at 26.1 ± 10.7 pA and the second peak was at 44.2 ± 19.6 pA. The long tail of the ΔI histogram can be fitted with a broad peak with a mean of 62.9 ± 50.1 pA, corresponding to the largest spikes.

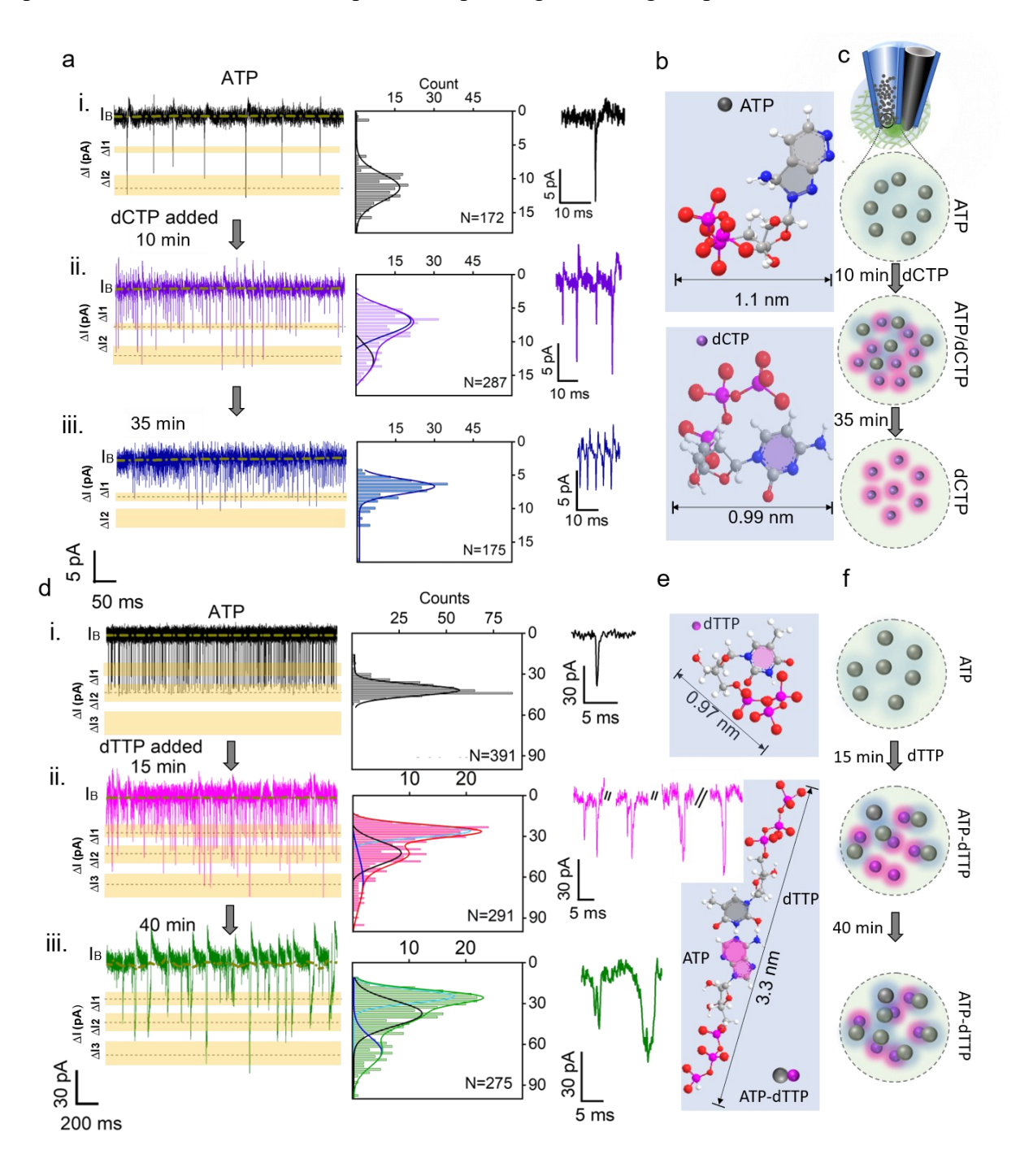


Figure 4. Probing intermolecular interactions between nucleoside triphosphates ATP and dCTP (a-c) and between ATP and dTTP (d-f). The initial concentrations of nucleoside triphosphates are always 100 pM and the applied V_{pore} remains at -20 mV. The *cis* side inside the nanopore barrel is 1xPBS and the *trans* side is fibrin hydrogel. The nanopore size is ~23 nm for results in a-c, and ~14 nm for results in e-f. a. Typical *i-t* traces for ATP alone (i), 10 min (ii), and 38 min (iii) after adding dCTP. Corresponding ΔI histograms of current spikes are shown next to the *i-t* traces. The solid lines represent the Gaussian fits to the histograms. The zoomed-in typical spikes are shown on the right side. b. Molecular structures of ATP and dCTP drawn by Chem3D after energy minimization. c. Schematic diagrams to illustrate the level of crowding of ATP and mixture of ATP with dCTP. d. Typical *i-t* traces for ATP alone (i), 15 min (ii), and 40 min (iii) after adding dTTP. Histograms of ΔI of current spikes are presented next to the corresponding *i-t* traces. The zoomed-in views of typical spikes are presented on the right side. e. Molecular structures of dTTP and hydrogen bonded ATP-dTTP complex. f. Schematic diagrams to show the formation of ATP-dTTP complexes.

These spikes are attributed to the formation of hydrogen-bonded ATP-dTTP complexes. Some of the current spikes in the i-t trace display two spikes in proximity, further indicating the presence of interacting pairs. After 40 min of recording, the event rate decreased (44 s⁻¹), but the percentage of the largest spikes obviously increased (see trace (iii) and histogram (iii)), suggesting that more ATP-dTTP complexes were formed. We have waited for more than 1 hr but we still did not observe a single distribution in ΔI . The notably different results between the ATP/dTTP mixture and ATP/dCTP mixture demonstrate that crowding can promote specific interactions between closely spaced molecules.

Considering the same charge and small size difference between ATP and dCTP or dTTP (see Figures 4b and e), it is surprising to observe the significant difference in ΔI . In our repeated measurements, we have noticed that the dCTP and dTTP are difficult to be detected alone and their spikes are always CEs when mixing with ATP (see Figure 4 and Figure S14). Meanwhile, the spikes of ATP always appear as CEs or BEs but not REs (see Figure S14). Therefore, these molecules are mainly detected in a more crowded environment. The more crowded environment thus enables a bigger difference in ΔI , which may have originated from the different interactions between moving ATP and surroundings in a jammed environment. The detailed mechanism still needs further investigation. Anyway, this phenomenon points in a new direction to enhance selectivity for label-free detection. Compared with ATP, guanosine triphosphate (GTP, 523 Da)

have stronger self-interactions and can interact with each other through Hoogsteen hydrogen bonds and form stable assemblies such as quadruplex structures.³⁵ We used the V_{pore} to modulate the

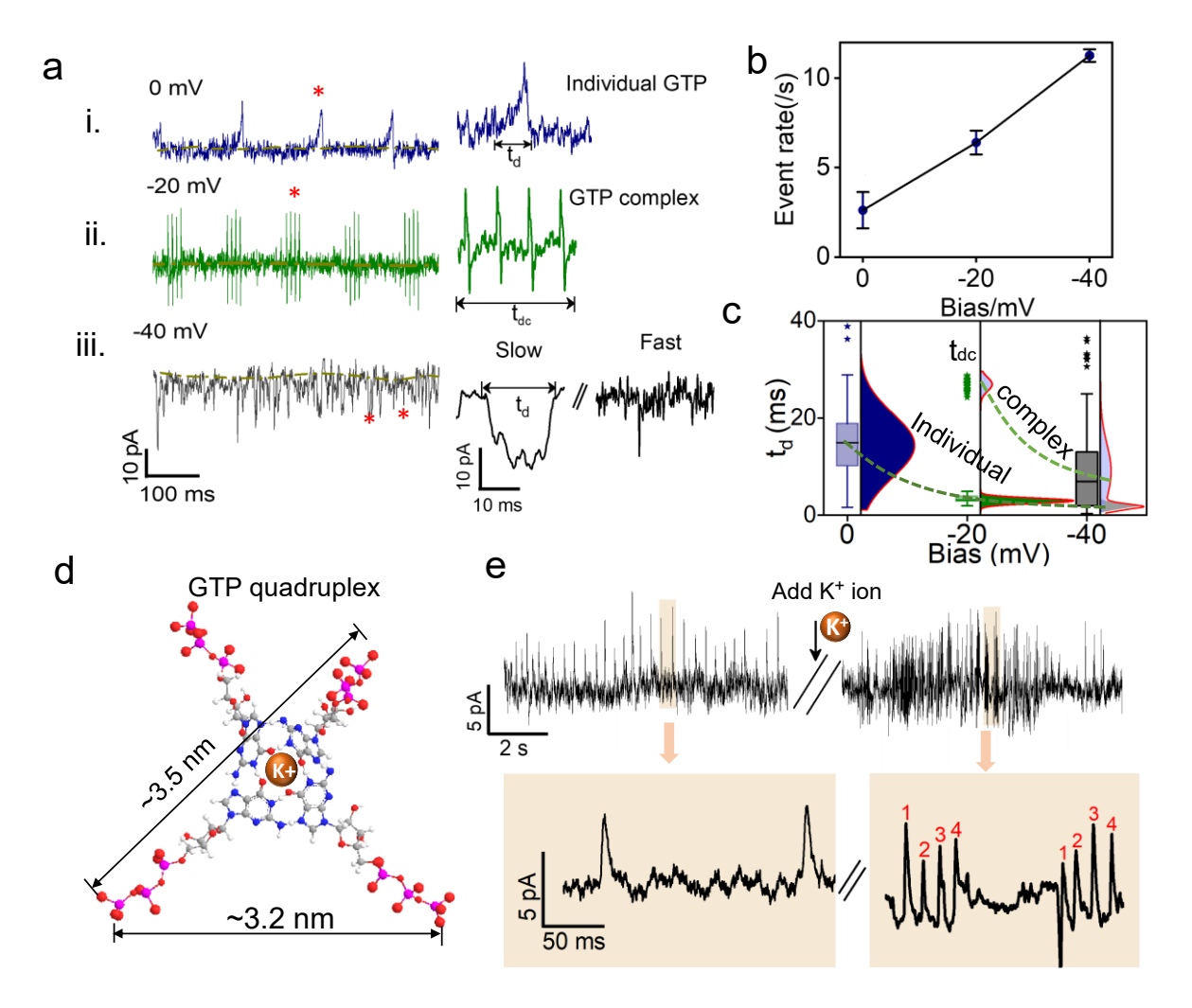


Figure 5. Probing self-interactions between jam-packed GTP. The size of the nanopore is \sim 18 nm. The initial GTP concentration is 500 pM. a. Representative *i-t* traces at different V_{pore} biases. Zoomed in traces showing individual current spikes are on the right side next to the corresponding *i-t* traces. b. Event rate at different V_{pore} . The error bars were calculated based on the standard deviation of at least 3 different clusters. The dash line serves as a visual guide. c. Box normal plot of t_d at different V_{pore} biases. d. Molecular structure of a G-quartet. The structure is drawn by chem3D software after energy minimization. e. *i-t* traces before and after adding potassium ion at the *cis* side. Zoomed-in traces are presented below the corresponding *i-t* traces.

degree of crowding at the nanopipette tip and, consequently, the interactions between GTP. Different from ATP, we observed more dynamic and less uniform shape changes for the current spikes, which is attributed to the stronger self-interactions of GTP and a higher heterogeneity in

local molecular density. As shown in Figures 5a and 5b, when the V_{pore} is more negative, the event rate increases, suggesting the crowding level increases. Correspondingly, the spike shapes transition from monophasic upward REs at zero bias to biphasic at -20 mV and monophasic downward CEs at -40 mV. Interestingly, at -20 mV, current spikes appear in small groups (see Figure 5a(ii)). About 80-90% of the groups contain four spikes. We attribute the origin of these spikes in a group of four to the formation of G-quartet complexes (see Figure 5d). ³⁶ The formation of spikes in a small group always has been repeatedly observed in the GTP only experiments but never in the ATP only experiments. Although the number of spikes in a group appears much more often as 4, the number can vary from 3 to 7, likely depending on the local crowding level and packing structure of GTP. At -40 mV, the spikes are very dense in the trace but can be generally divided into two groups: slow and fast events. The fast spikes are like the spikes observed at zero and -20 mV and are attributed to the translocation of individual GTP. The slow spikes show a much bigger duration time, which is attributed to the translocation events of GTP complexes. This is supported by the fact that we have observed the dynamic transition from a small group of spikes with small t_d to a merged peak with bigger t_d in one trace (see Figure S15). We have also conducted experiments with a higher bias. Even denser spikes were observed at -100 mV with many grouped spikes (see Figure S15). Figure 5c shows the change of t_d as a function of V_{pore}. Two peaks are observed for the t_d distribution at -40 mV, which is attributed to the existence of slow and fast spikes. Considering the slow spikes are likely from the GTP complex, we also include t_{dc} of small clusters (as defined in Figure 5a(ii)) for the data at -20 mV. In this way, we can see the continuous decrease of translocation time of individual GTP or GTP complex with the increase of V_{pore} magnitude.

The hydrogen-bonded GTP assemblies are often stabilized by centrally coordinated potassium ions (see Figure 5d).³⁷ We thus examined the possibility of GTP assemblies with and without potassium ions. As shown in Figure 5e, the small group formation of spikes cannot be observed initially without potassium ions in the solution but appears after adding potassium ions to the solution inside the nanopipette nanopore barrel.

Conclusion

In summary, we have successfully demonstrated a novel approach to enable the nanopipette to achieve an unprecedented sensitivity for the detection of small molecules at the single-molecule level by maximizing the nano-confinement effect of the nanopipette tip. By hindering the exit of

small molecules using viscous hydrogel at the trans side, the nanopipette tip can be jammed with molecules. The jammed nanopipette tip creates a smaller nanopore. However, the effect of molecular jamming is not just reducing the volume of nanopore, but also displacing ions and further reducing the mobilities of ions and molecules. The slowed movement of molecules and ions leads to a high SNR for current spikes and the enriched molecules lead to a high event rate. The ion concentration variation also induces rich and dynamic variations in the ionic current signals, providing valuable information on the local crowding level. This approach proves particularly advantageous for detecting small biomolecules as their higher mobility allows them for effective and fast enrichment at the tip even without applying any bias. Implementing nanopipettes with pore sizes larger than 10-15 nm, we have achieved high throughput detection of small biomolecules in the size range of approximately one to a few nanometers under physiological conditions. By introducing noninteracting larger molecules to enhance the volume exclusion effect at the cis side inside the nanopipette, small molecules more than ten times smaller than the pore size can still be effectively enriched and detected. Furthermore, this novel approach enables the nanopipette to function as a nano-reactor for investigating intermolecular interactions among small biomolecules in a crowded environment. As a model system, the interactions of nucleosides triphosphate have been successfully probed. We also observed the enhanced molecular recognition capability to differentiate different nucleoside triphosphates. Although the detailed mechanism still needs further investigation, we believe the concept of jamming molecules in the nanopipette tip to improve molecule sensitivity is a significant advancement for the nanopipette-based nanopore sensor. The approach is simple, inexpensive, and requires no further modification. With its versatility and promising capabilities, we anticipate that this new method will find diverse applications and open new avenues for scientific exploration, such as small molecule counting and detection, biomolecule stereochemistry, oligomerization, and interaction dynamics.

Experimental Setup and Measurement.

Reagent and Material. Equine spleen ferritin (ferritin), BSA, insulin, and lysozyme from chicken egg white, nisin, PEG 8000 (89510), MP-11, ATP, GTP, dTTP, dCTP, and FITC dye used in the experiments were purchased from the Millipore Sigma. All the molecule solutions were prepared in 1xPBS with the typical concentration in the range from 100 to 500 pM. The 1xPBS solution (pH 7.4) was prepared by dissolving PBS powder (8.0 g of NaCl, 2.89 g of NaHPO₄.2H₂O, 0.2 g of

KCL, 0.2 g of KH₂PO₄) in 1 L of deionized (DI) water. All solutions were prepared using DI water (~18 MΩ) (LabChem, ACS Reagent Grade, ASTM Type I).

The Fabrication and Characterization of Multifunctional Nanopipette. Following the previous report, the multifunctional nanopipettes were fabricated from quartz theta capillary tubes (FG-QT120-90-7.5, Sutter instrument).³⁸ In brief, the quartz theta pipettes were first cleaned by piranha solution (Sulfuric acid and hydrogen peroxide in the volume ratio 3:1) and then pulled by a laser puller (P-2000, shutter Instrument) with the following parameters: Heat= 825, FIL=3, VEL= 220, PUL=190. Then one of the barrels was filled with pyrolytic carbon to form the CNE.³⁸ The nanopore size was estimated based on the measured ionic conductance from the current-voltage (*i-v*) plots (see Figure S1). Depending on the size of tested biomolecules, the diameters of the prepared nanopipette nanopores are in the range of 15-70 nm. The effective surface area of CNE was estimated from the cyclic voltammogram (CV), which is in the range of 0.15-0.9 μ m² with an average effective surface area of ~0.3 μ m². It is important to note that the CNE is not required for this approach. We primarily utilized CNE as a complementary detection method to probe changes in the local electrostatic environment.

Experimental Setup. The molecules are loaded from the backend of a nanopore barrel of a long taper quartz single-barrel or dual-barrel nanopipette (see Figure 1a). The typical volume for a load is 7-11μL. After loading, we typically wait for 1-2 hr for small molecules and 3-5 hr for larger proteins before measurements. The ionic current-time (*i-t*) and potential-time (*v-t*) were recorded using an experimental setup as illustrated in Figure 1a. The electrochemical measurement was performed using an Axopatch 200B amplifier (Molecular Devices Inc., CA). Freshly prepared Ag/AgCl wires were used as the electrodes and a battery-powered high-impedance differential amplifier was used to measure the open-circuit potential of the CNE. The bandwidth of the low pass filter is 5 kHz for current and 40 kHz for potential signals. The data were recorded by Yokogawa oscilloscope (DL850) with a sampling rate of 50 kHz. All experiments and measurements were performed at room temperature.

Fibrin Hydrogel Fabrication and Characterization. Sterile fibrinogen from human plasma (Millipore Sigma, F3879) was dissolved in 1xPBS at 35 mg/ml and kept at 37°C for about two hours. Thrombin from human plasma (Millipore Sigma, 9002044) was dissolved in 1x PBS at 100 U/ml. Thrombin solution was then added to the fibrinogen solution with a 1:3 ratio by volume at

37°C. The mixture of about 100 μL was left in a small PDMS chamber for about 20 min to form

the hydrogel. We then added about 20 µL of 1xPBS solution to the surface of the hydrogel. The

topography images of fibrin hydrogel were collected by AFM (XE-Bio system, Park system Inc

Santa, CA) in tapping mode with cantilevers whose stiffness was 0.4 N/m. To prepare the sample

for AFM imaging, a few drops of freshly prepared fibrin hydrogel (~30 μl) are dried on the freshly

cleaved mica surface for 10-20 min.

Data Reproducibility and Analysis. To guarantee the reproducibility of the results, the

measurements for each biomolecule have been repeated by at least three nanopipettes. The ionic

current and potential data were analyzed by using custom programs written in LabVIEW and

OriginPro 2018b. The moving average smoothing method with a 2 ms time window is typically

applied to the data before statistical analysis. ImageJ was used to analyze the AFM and

fluorescence images.

ASSOCIATED CONTENT

Data Availability Statement

All the relevant data are available with the article and the Supplementary information files, or

available from the corresponding author upon reasonable request.

Supporting information

The Supplementary Information is available free of charge via the Internet at

https://pubs.acs.org/doi/xxx.

Nanopipette fabrication and characterization; Viscosity measurement; Hydrodynamic radii, diffusion constants and mobilities of tested molecules; Fluorescence imaging setup; Measurements with PEG-8k; Large protein results in Fibrin Hydrogel; Nisin detection in fibrin hydrogel; MP-11 results at -30 mV and analysis of noise spectral density; Ferritin results; Use of other large proteins to enhance the detection of insulin; Extra data for the detection of ATP and dTTP interaction; Extra

data for GTP.

AUTHOR INFORMATION

Corresponding Author

Jin He: Department of Physics, Biomolecular Science Institute, Florida International University,

Miami, FL 33199, USA; orcid.org/0000-0002-2633-9809

E-mail: jinhe@fiu.edu.

Authors:

Santosh Khatri: Department of Physics, Florida International University, Miami, FL 33199,

USA; https://orcid.org/0000-0001-5305-3294

19

Popular Pandey: Department of Physics, Florida International University, Miami, FL 33199, USA;

German Mejia: Department of Physics, Biomolecular Science Institute, Florida International University, Miami, FL 33199, USA;

Fenfei Leng: Department of Physics, Biomolecular Science Institute, Florida International University, Miami, FL 33199, USA;

Notes

The authors declare no competing financial interest in association with this study.

Acknowledgments

This work was supported by NSF 2216824 and NIH 1R01HL160740 (to J.H.) and NIH grants 1R21AI125973 and 1R21AI178134 (to F.L.). Popular acknowledges the support of the FIU CASE outstanding postdoc fellowship. We acknowledge Zhe Wang for the help of preparing figures.

References:

- (1) Neher, E.; Sakmann, B. Single-channel currents recorded from membrane of denervated frog muscle fibres. *Nature* **1976**, *260* (5554), 799-802, DOI: 10.1038/260799a0.
- (2) Kasianowicz, J. J.; Brandin, E.; Branton, D.; Deamer, D. W. Characterization of individual polynucleotide molecules using a membrane channel. *Proceedings of the National Academy of Sciences* **1996**, *93* (24), 13770-13773, DOI: 10.1073/pnas.93.24.13770.
- (3) Bayley, H.; Cremer, P. S. Stochastic sensors inspired by biology. *Nature* **2001**, *413* (6852), 226-230, DOI: 10.1038/35093038.
- (4) Howorka, S.; Siwy, Z. Nanopore analytics: sensing of single molecules. *Chemical Society Reviews* **2009**, *38* (8), 2360-2384.
- (5) Muthukumar, M.; Plesa, C.; Dekker, C. Single-molecule sensing with nanopores. *Physics Today* **2015**, *68* (8), 40-46, DOI: 10.1063/PT.3.2881.
- (6) Shi, W.; Friedman, A. K.; Baker, L. A. Nanopore Sensing. *Anal. Chem.* **2017**, *89* (1), 157-188, DOI: 10.1021/acs.analchem.6b04260.
- (7) Ying, Y.-L.; Hu, Z.-L.; Zhang, S.; Qing, Y.; Fragasso, A.; Maglia, G.; Meller, A.; Bayley, H.; Dekker, C.; Long, Y.-T. Nanopore-based technologies beyond DNA sequencing. *Nature Nanotechnology* **2022**, *17* (11), 1136-1146, DOI: 10.1038/s41565-022-01193-2.
- (8) Deamer, D.; Akeson, M.; Branton, D. Three decades of nanopore sequencing. *Nat. Biotechnol.* **2016**, 34 (5), 518-524, DOI: 10.1038/nbt.3423.
- (9) Wanunu, M. Nanopores: A journey towards DNA sequencing. *Physics of Life Reviews* **2012**, *9* (2), 125-158, DOI: https://doi.org/10.1016/j.plrev.2012.05.010.
- (10) Ayub, M.; Hardwick, S. W.; Luisi, B. F.; Bayley, H. Nanopore-Based Identification of Individual Nucleotides for Direct RNA Sequencing. *Nano Lett.* **2013**, *13* (12), 6144-6150, DOI: 10.1021/nl403469r.
- (11) Plesa, C.; Kowalczyk, S. W.; Zinsmeester, R.; Grosberg, A. Y.; Rabin, Y.; Dekker, C. Fast Translocation of Proteins through Solid State Nanopores. *Nano Lett.* **2013**, *13* (2), 658-663, DOI: 10.1021/nl3042678.
- (12) Dekker, C. Solid-state nanopores. *Nature Nanotechnology* **2007**, *2* (4), 209-215, DOI: 10.1038/nnano.2007.27.

- (13) Yu, R.-J.; Ying, Y.-L.; Gao, R.; Long, Y.-T. Confined Nanopipette Sensing: From Single Molecules, Single Nanoparticles, to Single Cells. *Angewandte Chemie International Edition* **2019**, *58* (12), 3706-3714, DOI: https://doi.org/10.1002/anie.201803229.
- (14) Xue, L.; Yamazaki, H.; Ren, R.; Wanunu, M.; Ivanov, A. P.; Edel, J. B. Solid-state nanopore sensors. *Nature Reviews Materials* **2020**, *5* (12), 931-951, DOI: 10.1038/s41578-020-0229-6.
- (15) Wang, Y.; Kececi, K.; Mirkin, M. V.; Mani, V.; Sardesai, N.; Rusling, J. F. Resistive-pulse measurements with nanopipettes: detection of Au nanoparticles and nanoparticle-bound anti-peanut IgY. *Chem Sci* **2013**, *4* (2), 655-663, DOI: 10.1039/C2SC21502K.
- (16) Ellis, R. J. Macromolecular crowding: an important but neglected aspect of the intracellular environment. *Current opinion in structural biology* **2001**, *11* (1), 114-119.
- (17) Freedman, K. J.; Otto, L. M.; Ivanov, A. P.; Barik, A.; Oh, S.-H.; Edel, J. B. Nanopore sensing at ultra-low concentrations using single-molecule dielectrophoretic trapping. *Nature Communications* **2016**, *7* (1), 10217, DOI: 10.1038/ncomms10217.
- (18) Pandey, P.; Panday, N.; Chang, S.; Pang, P.; Garcia, J.; Wang, X.; Fu, Q.; He, J. Probing Dynamic Events of Dielectric Nanoparticles by a Nanoelectrode-Nanopore Nanopipette. *Chemelectrochem* **2018**, *5* (20), 3102-3112, DOI: 10.1002/celc.201800163.
- (19) Pandey, P.; Garcia, J.; Guo, J.; Wang, X.; Yang, D.; He, J. Differentiation of metallic and dielectric nanoparticles in solution by single-nanoparticle collision events at the nanoelectrode. *Nanotechnology* **2019**, *31* (1), 015503, DOI: 10.1088/1361-6528/ab4445.
- (20) Kim, D.; Sonker, M.; Ros, A. Dielectrophoresis: From Molecular to Micrometer-Scale Analytes. *Anal. Chem.* **2019**, *91* (1), 277-295, DOI: 10.1021/acs.analchem.8b05454.
- (21) Squires, A. H.; Hersey, J. S.; Grinstaff, M. W.; Meller, A. A Nanopore–Nanofiber Mesh Biosensor To Control DNA Translocation. *Journal of the American Chemical Society* **2013**, *135* (44), 16304-16307, DOI: 10.1021/ja408685x.
- (22) Waugh, M.; Carlsen, A.; Sean, D.; Slater, G. W.; Briggs, K.; Kwok, H.; Tabard-Cossa, V. Interfacing solid-state nanopores with gel media to slow DNA translocations. *ELECTROPHORESIS* **2015**, *36* (15), 1759-1767, DOI: https://doi.org/10.1002/elps.201400488.
- (23) Yoshida, H.; Goto, Y.; Akahori, R.; Tada, Y.; Terada, S.; Komura, M.; Iyoda, T. Slowing the translocation of single-stranded DNA by using nano-cylindrical passage self-assembled by amphiphilic block copolymers. *Nanoscale* **2016**, *8* (43), 18270-18276, DOI: 10.1039/C6NR06575A.
- (24) Acharya, S.; Jiang, A.; Kuo, C.; Nazarian, R.; Li, K.; Ma, A.; Siegal, B.; Toh, C.; Schmidt, J. J. Improved Measurement of Proteins Using a Solid-State Nanopore Coupled with a Hydrogel. *ACS Sensors* **2020**, *5* (2), 370-376, DOI: 10.1021/acssensors.9b01928.
- (25) Nazarian, R.; Lee, E.; Siegel, B.; Kuo, C.; Acharya, S.; Schmidt, J. Quantitative Measurements of Protein Volume and Concentration using Hydrogel-Backed Nanopores. *ACS Sensors* **2021**, *6* (3), 722-726, DOI: 10.1021/acssensors.1c00284.
- (26) Chau, C. C.; Radford, S. E.; Hewitt, E. W.; Actis, P. Macromolecular Crowding Enhances the Detection of DNA and Proteins by a Solid-State Nanopore. *Nano Lett.* **2020**, *20* (7), 5553-5561, DOI: 10.1021/acs.nanolett.0c02246.
- (27) Al Sulaiman, D.; Gatehouse, A.; Ivanov, A. P.; Edel, J. B.; Ladame, S. Length-Dependent, Single-Molecule Analysis of Short Double-Stranded DNA Fragments through Hydrogel-Filled Nanopores: A Potential Tool for Size Profiling Cell-Free DNA. *ACS Applied Materials & Interfaces* **2021**, *13* (23), 26673-26681, DOI: 10.1021/acsami.1c01145.
- (28) Nouri, R.; Tang, Z.; Guan, W. Quantitative Analysis of Factors Affecting the Event Rate in Glass Nanopore Sensors. *ACS Sensors* **2019**, *4* (11), 3007-3013, DOI: 10.1021/acssensors.9b01540.
- (29) Liang, S.; Xiang, F.; Tang, Z.; Nouri, R.; He, X.; Dong, M.; Guan, W. Noise in nanopore sensors: sources, models, reduction, and benchmarking. *Nanotechnology and Precision Engineering* **2020**, *3* (1), 9-17.

- (30) Qiu, Y.; Vlassiouk, I.; Chen, Y.; Siwy, Z. S. Direction Dependence of Resistive-Pulse Amplitude in Conically Shaped Mesopores. *Anal. Chem.* **2016**, *88* (9), 4917-4925, DOI: 10.1021/acs.analchem.6b00796. (31) Lan, W.-J.; Holden, D. A.; Zhang, B.; White, H. S. Nanoparticle Transport in Conical-Shaped Nanopores. *Anal. Chem.* **2011**, *83* (10), 3840-3847, DOI: 10.1021/ac200312n.
- (32) Chen, K.; Bell, N. A.; Kong, J.; Tian, Y.; Keyser, U. F. Direction-and salt-dependent ionic current signatures for DNA sensing with asymmetric nanopores. *Biophysical journal* **2017**, *112* (4), 674-682.
- (33) Smeets, R. M. M.; Keyser, U. F.; Krapf, D.; Wu, M.-Y.; Dekker, N. H.; Dekker, C. Salt Dependence of Ion Transport and DNA Translocation through Solid-State Nanopores. *Nano Lett.* **2006**, *6* (1), 89-95, DOI: 10.1021/nl052107w.
- (34) Lastra, L. S.; Bandara, Y. M. N. D. Y.; Nguyen, M.; Farajpour, N.; Freedman, K. J. On the origins of conductive pulse sensing inside a nanopore. *Nature Communications* **2022**, *13* (1), 2186, DOI: 10.1038/s41467-022-29758-8.
- (35) Nasiri, A. H.; Wurm, J. P.; Immer, C.; Weickhmann, A. K.; Wöhnert, J. An intermolecular G-quadruplex as the basis for GTP recognition in the class V-GTP aptamer. *Rna* **2016**, *22* (11), 1750-1759, DOI: 10.1261/rna.058909.116.
- (36) Kogut, M.; Kleist, C.; Czub, J. Molecular dynamics simulations reveal the balance of forces governing the formation of a guanine tetrad-a common structural unit of G-quadruplex DNA. *Nucleic Acids Res* **2016**, 44 (7), 3020-3030, DOI: 10.1093/nar/gkw160.
- (37) Bhattacharyya, D.; Mirihana Arachchilage, G.; Basu, S. Metal Cations in G-Quadruplex Folding and Stability. *Front Chem* **2016**, *4*, 38, DOI: 10.3389/fchem.2016.00038.
- (38) Panday, N.; Qian, G.; Wang, X.; Chang, S.; Pandey, P.; He, J. Simultaneous Ionic Current and Potential Detection of Nanoparticles by a Multifunctional Nanopipette. *ACS Nano* **2016**, *10* (12), 11237-11248, DOI: 10.1021/acsnano.6b06307.

TOC

